Spatial organization of single mRNPs at different stages of the gene expression pathway

Srivathsan Adivarahan[1], Samir Rahman[1] and Daniel Zenklusen[1]*

Affiliations:

(1) Département de Biochimie et médecine moléculaire, Université de Montréal, Montréal, Québec, Canada

***Corresponding author: daniel.r.zenklusen@umontreal.ca**

Abstract

mRNAs form ribonucleoprotein complexes (mRNPs) by association with proteins that are crucial for mRNA metabolism. While the mRNP proteome has been well characterized, little is known about mRNP organization. Using a single molecule approach, we show that mRNA conformation changes depending on its cellular localization and translational state. Compared to nuclear mRNPs, translation decompacts individual mRNAs, consistent with formation of polysomes, while their sequestration into stress-granules leads to increased compaction. Moreover, translating mRNAs rarely show co-localizing 5' and 3' ends, indicating that mRNAs are either not translated in a closed-loop configuration, or that mRNA circularization is transient, suggesting that a stable closed-loop conformation is not a universal state for all translating mRNAs.

One Sentence Summary: Single mRNA studies in cells show RNA compaction changes depending on translational state, but mRNAs are not translated in closed-loop conformation.

Main text

mRNAs are single-stranded nucleic acid polymers. Intramolecular base pairing and binding of RNA binding proteins (RBPs), many of which contain homo and hetero-dimerization domains, assemble mRNAs into mRNPs (*1*). Yet how mRNPs are organized as three-dimensional particles within cells remains unknown (*2-10*). mRNPs may exist as compact assemblies or as flexible open polymers allowing frequent interactions between different regions required to regulate mRNA metabolisms at different stages of the gene expression pathway, such as during translation or RNA turnover (*11-13*). To study mRNP organization within cells, we combined Structured Illumination Microscopy (SIM) with single molecule resolution fluorescent in situ hybridization (smFISH) and Gaussian fitting to investigate the spatial relationship of various regions within mRNAs in different cellular compartments and translational states.

To determine if this approach allows to spatially resolve different regions within single mRNAs, we first measured co-localization precision by hybridizing alternating probes, labeled with cy3 and cy5, to a 1.2 kb region within the 18,413 nt-long MDN1 mRNA in paraformaldehyde-fixed HEK293 cells. Images were acquired spanning the entire cell volume, and 3D datasets reduced to 2D by maximum intensity projection. Figure 1A shows co-localization of signals emitted from both channels detecting single MDN1 mRNAs. We determined the center of each signal by 2D Gaussian fitting and measured the distance between signals from both channels (*14*, *15*). We obtained a co-localization precision of 21 nm, indicating that we can resolve discrete regions within mRNAs separated by more than 20 nm (Fig. 1C). We then positioned labeled probes to the 5' and 3' ends of MDN1 to determine maximal extension of the MDN1 mRNA in cells (Fig S1 and Table S2), which, fully extended, would measure 5.5 μm in length. Upon analyzing

cytoplasmic mRNAs, we observed few overlapping 5' and 3' signals; however, the majority of 5' signals had a 3' signal within close proximity (Fig 1B), and further measurements of 5'-3' distances revealed separation of the two signals up to 300 nm. To determine if 5' and 3' signals were part of the same mRNA molecule, we used a third set of FISH probes tiling the entire length of the mRNA between the 5' and 3' regions in 500 nt intervals. The tiling signal overlapped with either one of the two regions, and connected the 5' and 3' within the 300 nm radius, confirming that 5' and 3' end signals belonged to the same molecule and, moreover, pointing towards an elongated conformation of cytoplasmic MDN1 mRNPs (Fig 1D). To better understand the spatial relationship between different regions within these mRNAs, we replaced the tiling probes with a probe set hybridizing to the middle region of the MDN1 mRNA (Fig 1E). Using these probes, we observed cytoplasmic mRNAs in various configurations in which the three different regions could be spatially resolved (Fig 1E and F). To measure the average volume of these cytoplasmic mRNAs, we aligned individual mRNAs using their center of mass and found a mean radius of gyration ($<R_g>$) of 73.95 nm (Fig 1G).

To determine whether such open conformations are particular to the long MDN1 mRNA or are a more common feature of cytoplasmic mRNAs, we measured compaction of two shorter mRNAs encoding for the splicing factor PRPF8 (7,445 nt) and the DNA polymerase alpha catalytic subunit POLA1 (5,486 nt). Similar to what was observed for MDN1, 5' and 3' ends of cytoplasmic POLA1 and PRPF8 mRNAs rarely co-localized (Fig S2A). Furthermore, end to end measurements showed a range of distances, although distributions were narrower than for MDN1, suggesting maximum expansion is limited by mRNA length. Together, these data show that cytoplasmic mRNAs exist in an open conformation where 5' and 3' are rarely found in close proximity.

Translating mRNPs are thought to exist in a closed-loop conformation where 5' and 3' ends of the mRNA are brought together through interactions between the cap binding eIF4F complex and the polyA binding protein PABPC1 (*11*, *12*, *16*). Surprisingly, 5'-3' conformations consistent with such a closed-loop configuration were rarely observed in our experiments. One possibility could be that most mRNAs with separated 5' and 3' ends are not in the process of being translated and that only the fraction with co-localizing ends represents the pool of translating mRNAs. If that were to be the case, interfering with translation should further reduce the fraction of mRNAs with co-localizing 5' and 3' ends. To test this hypothesis, we treated cells, prior to fixation, with drugs that affect translation via different mechanisms: cycloheximide interferes with translation by binding to the E-site of the 60S ribosomal unit and stabilizes polysomes, whereas puromycin causes premature chain termination and disassembles polysomes (*17*). Treatment with cycloheximide only minimally affected the percentage of co-localizing 5'-3' ends, and end-to-end distances showed a wide distribution similar to those observed in untreated cells (Fig 2C). However, the disassembly of polysomes following a short treatment with puromycin (10 min) resulted in an unexpected phenotype where the 5'-3' ends of most transcripts were found co-localizing (Fig 2A). Distance measurements showed a narrow distribution with a median of 36 nm. Similarly, POLA1 and PRPF8 ends showed a high degree of co-localization with similar median 5'-3' end distances (Fig S2B and 2C). This observation could either represent a change in mRNP conformation resulting in increased levels of 5'-3' interaction, or it could be the result of a general compaction of the mRNP due to the loss of bound ribosomes. Probes hybridizing to the middle region of MDN1, or tiling probes along the entire length of the MDN1 transcript, showed that puromycin treatment resulted in a general compaction of the mRNPs (Fig 2B). Overlaying mRNA conformations revealed a much less extended form of these mRNPs compared to untreated cells

(Fig 2D and E). These observations suggest that most cytoplasmic mRNAs are translated, that mRNAs within translating mRNPs are not arranged in a stable closed-loop conformation, and translation inhibition leads to a compaction of these mRNPs.

Our data demonstrates that translation causes a decompaction of mRNPs and a separation of 5' and 3' regions of mRNAs. If translation is required for an open RNP conformation, non-translating RNAs, such as cytoplasmic long non-coding RNAs (lncRNAs) should show a similar level of compaction than non-translating mRNAs, and, moreover, their compaction should be unaffected by translation inhibitors. We therefore measured end-to-end distances for two lncRNAs, TUG1 (6,091 nt) and OIP5-AS1 (8,300 nt), which were previously found to be present in both the nucleus and the cytoplasm (*18*). Both lncRNAs contain short putative ORFs that could lead to their association with ribosomes, however, their translation will be limited to the very 5' of their RNA (*19*). As shown in Fig 3A, 5' and 3' labeled TUG1 and OIP5-AS1 lncRNAs displayed a more compact conformation compared to the similarly sized PRPF8 mRNA. In addition, 5'-3' distances of TUG1 and OIP5-AS1 lncRNAs were unaffected by puromycin, further suggesting that decompaction of cytoplasmic mRNAs requires the formation of polysomes (Fig 3B).

If eviction of ribosomes from translating mRNAs by puromycin results in a strong compaction of mRNA, mRNAs that are translationally repressed in response to external stimuli or environmental triggers should also acquire a compact conformation. Treatment with sodium arsenite inhibits translation through phosphorylation of eIF2α and results in disassembly of polysomes and sequestration of mRNAs in stress granules (*20*, *21*). We found that upon induction of stress granule assembly in U2OS cells, following treatment with arsenite for 1 hour, cytoplasmic MDN1 mRNAs did not only relocate to stress granules, but also show a highly compact conformation, as observed using 5'- 3' and tiling probes (Fig 3C). End-to-end measurements

showed a level of mRNA compaction similar to that seen in puromycin-treated cells, and similar compaction was also observed for POLA1 and PRPF8 mRNAs under the same conditions (Fig S3A). Interestingly, not all mRNAs accumulated in stress granules; however, most mRNAs that remained outside showed the same level of compaction than those within, suggesting that translation inhibition occurs independently of mRNA sequestration to stress granules, as previously suggested (*20*). Moreover, a fraction of TUG1 and OIP5-AS1 was also found localized to stress granules, and this localization did not alter their compaction (Fig S3B).

We then asked whether the compacted state of mRNAs found within stress granules, or after puromycin treatment, reflects a default state for non-translating cellular mRNPs. In the nucleus, nascent mRNAs are co-transcriptionally spliced and assembled into mRNPs resulting in the binding of a large set of RBPs, including the exon-junction complex and SR proteins (*2*, *22*, *23*). During translation in the cytoplasm, many RBPs bound to the open reading frame are evicted by the ribosome. mRNAs that have been translated and then go into a translationally silent state might therefore be bound by fewer proteins than cytoplasmic mRNAs prior to their first round of translation or nuclear mRNPs before their export to the cytoplasm. To therefore determine whether a default compaction state exists for non-translating mRNPs, we investigated the organization of nuclear MDN1 mRNAs. Compared to MDN1 mRNAs in stress granules, many nuclear MDN1 mRNAs were found in an extended conformation, yet more compacted than translating cytoplasmic mRNAs (Fig. 4A-E). Importantly, open mRNP conformations of nuclear MDN1 were not sensitive to puromycin treatment (Fig S4), suggesting that assembly of nuclear mRNPs results in more extended mRNP compared to translationally inhibited mRNPs.

Electron microscopy (EM) studies visualizing the 35 kb-long nuclear Balbiani ring mRNPs in the dipteran *Chironomus tentans* have suggested that nuclear mRNPs exist as compact particles

with 5' and 3' ends in close proximity (*3*). Our observations do not support such a globular structure, but instead are consistent with EM images of purified nuclear mRNPs from yeast, which suggest that mRNAs assemble in a linearly compacted polymer that can exist in various states of compaction (*4*).

The current model suggests translation occurring in a closed-looped configuration is based on biochemical characterization of PABC1 and eIF4F interactions, and supported by EM images of *in vitro* assembled close-looped mRNPs (*11*, *12*, *16*, *24*, *25*). On the other hand, studies investigating polysome conformation by EM *in vivo*, have observed polysomes in various conformations with only some compatible with a closed-loop translation model (*7*, *26*). However, as mRNA was not visualized in these polysomes, it was not possible to assess 5' -3' end mRNA interactions based on those EM images. Overall, our data suggest that, at least for some mRNAs, translation does not occur in a stable closed loop conformation, and future studies will have to determine whether this is true for all mRNAs.

Regulatory elements in mRNAs are often located within the 3'UTR and modulate processes at the 5' end, such as de-capping or translation initiation (*13*, *25*). Signal transmission from the 3' to the 5' likely requires a flexible RNA polymer that allows both ends to meet. However, we have little understanding of the biophysical properties of mRNPs *in vivo*. Understanding whether the open conformations observed here for mRNAs reflect continuously changing, dynamic conformations that result in frequent transient 5'-3'end interactions, and to determine if the biophysical properties of mRNAs and mRNPs allow frequent inter-molecular interactions in general, will require new tools that allow us to study mRNP organization within cells in real time.

References

1. G. Singh, G. Pratt, G. W. Yeo, M. J. Moore, The Clothes Make the mRNA: Past and Present Trends in mRNP Fashion. *Annual Review of Biochemistry*. **84**, 325–354 (2015).

2. G. Singh *et al.*, The Cellular EJC Interactome Reveals Higher-Order mRNP Structure and an EJC-SR Protein Nexus. *Cell* (2012), doi:10.1016/j.cell.2012.10.007.

3. H. Mehlin, B. Daneholt, U. Skoglund, Structural interaction between the nuclear pore complex and a specific translocating RNP particle. *J Cell Biol*. **129**, 1205–1216 (1995).

4. J. Batisse, C. Batisse, A. Budd, B. Böttcher, E. Hurt, Purification of nuclear poly(A)-binding protein Nab2 reveals association with the yeast transcriptome and a messenger ribonucleoprotein core structure. *J Biol Chem*. **284**, 34911–34917 (2009).

5. M. A. Skabkin *et al.*, Structural organization of mRNA complexes with major core mRNP protein YB-1. *Nucleic Acids Res*. **32**, 5621–5635 (2004).

6. J. Rech, An Ultrastructural Characterization of in Vitro-Assembled hnRNP C Protein-RNA Complexes. *J. Struct. Biol.* **114**, 84–92 (1995).

7. F. Brandt, L.-A. Carlson, F. U. Hartl, W. Baumeister, K. Grünewald, The three-dimensional organization of polyribosomes in intact human cells. *Mol Cell*. **39**, 560–569 (2010).

8. Z. A. Afonina, A. G. Myasnikov, V. A. Shirokov, B. P. Klaholz, A. S. Spirin, Conformation transitions of eukaryotic polyribosomes during multi-round translation. *Nucleic Acids Res*. **43**, 618–628 (2015).

9. V. Ramani, R. Qiu, J. Shendure, High-throughput determination of RNA structure by proximity ligation. *Nat Biotechnol*. **33**, 980–984 (2015).

10. Z. Lu *et al.*, RNA Duplex Map in Living Cells Reveals Higher-Order Transcriptome Structure. *Cell*. **165**, 1267–1279 (2016).

11. S. Z. Tarun, Sachs, AB, Association of the yeast poly(A) tail binding protein with translation initiation factor eIF-4G. *The EMBO Journal*. **15**, 7168–7177 (1996).

12. H. Imataka, A. Gradi, N. Sonenberg, A newly identified N-terminal amino acid sequence of human eIF4G binds poly(A)-binding protein and functions in poly(A)-dependent translation. *The EMBO Journal*. **17**, 7480–7489 (1998).

13. M. R. Fabian, N. Sonenberg, The mechanics of miRNA-mediated gene silencing: a look under the hood of miRISC. *Nat Struct Mol Biol*. **19**, 586–593 (2012).

14. R. Thompson, D. Larson, W. Webb, Precise nanometer localization analysis for individual fluorescent probes. *Biophys J*. **82**, 2775–2783 (2002).

15. D. Zenklusen, D. R. Larson, R. H. Singer, Single-RNA counting reveals alternative modes of gene expression in yeast. *Nat Struct Mol Biol*. **15**, 1263–1271 (2008).

16. S. Wells, P. Hillner, R. Vale, A. Sachs, Circularization of mRNA by eukaryotic translation initiation factors. *Mol Cell*. **2**, 135–140 (1998).

17. M. Bhat *et al.*, Targeting the translation machinery in cancer. *Nature Reviews Drug Discovery*. **14**, 261–278 (2015).

18. M. N. Cabili *et al.*, Localization and abundance analysis of human lncRNAs at single-cell and single-molecule resolution. *Genome Biology*. **16**, 20 (2015).

19. S. van Heesch *et al.*, Extensive localization of long noncoding RNAs to the cytosol and mono- and polyribosomal complexes. *Genome Biol*. **15**, R6 (2014).

20. M. D. Panas, P. Ivanov, P. Anderson, Mechanistic insights into mammalian stress granule dynamics. *J Cell Biol*. **215**, 313–323 (2016).

21. J. R. Buchan, R. Parker, Eukaryotic stress granules: the ins and outs of translation. *Mol Cell*. **36**, 932–941 (2009).

22. H. Le Hir, E. Izaurralde, L. E. Maquat, M. J. Moore, The spliceosome deposits multiple proteins 20–24 nucleotides upstream of mRNA exon–exon junctions. *The EMBO Journal*. **19**, 6860–6869 (2000).

23. M. Müller-McNicoll, K. M. Neugebauer, How cells get the message: dynamic assembly and function of mRNA-protein complexes. *Nature Reviews Genetics*. **14**, 275–287 (2013).

24. T. Nishimura, M. R. Fabian, Scanning for a unified model for translational repression by microRNAs. *The EMBO Journal*. **35**, 1158–1159 (2016).

25. O. S. Rissland, The organization and regulation of mRNA–protein complexes. *WIREs RNA* (2016), doi:10.1002/wrna.1369.

26. A. K. Christensen, C. M. Bourne, Shape of large bound polysomes in cultured fibroblasts and thyroid epithelial cells. *The Anatomical Record*. **255**, 116–129 (1999).

Acknowledgement

We thank Marlene Oeffinger, Nicole Francis, Olivia Rissland and Steve Michnick for critical discussion and reading of the manuscript. This work has been supported CIHR (Project Grant-366682), FRQ-S (Chercheur-boursier Junior 2) and CFI.

Figures

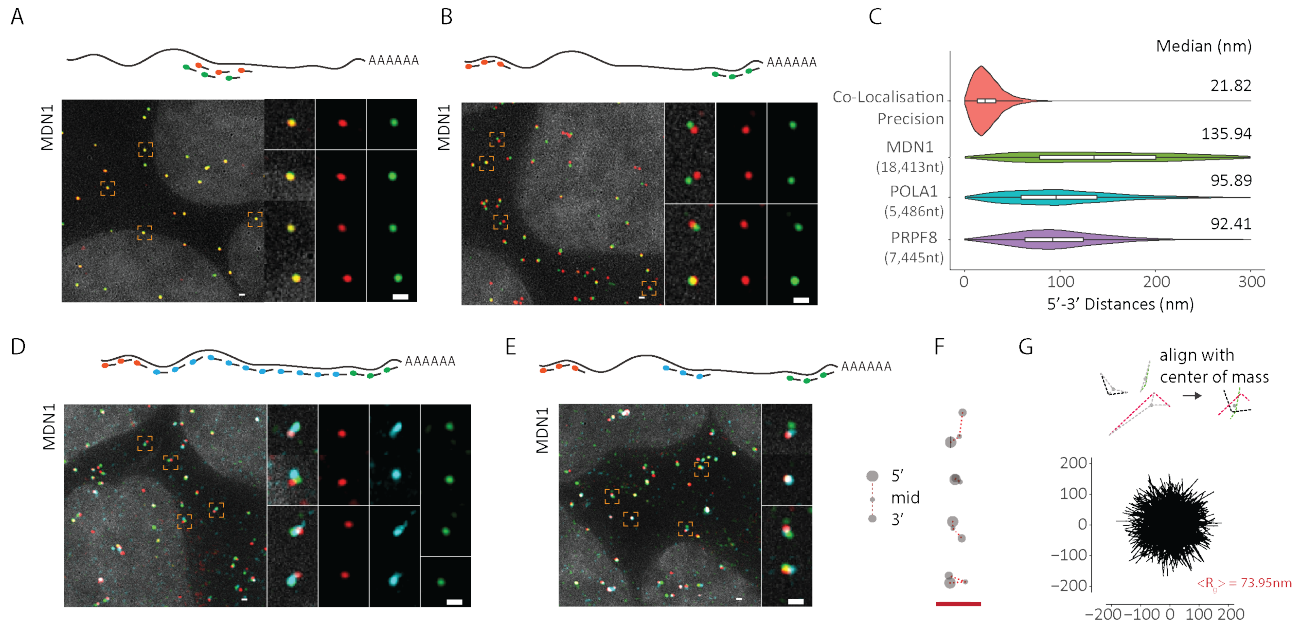

Adivarahan et al. Figure 1

Figure 1: Visualizing single mRNA reveals open conformations of cytoplasmic mRNAs. **(A)** smFISH images using alternating probes labeled in cy3 (red) and cy5 (green) to middle region of MDN1 mRNA in paraformaldehyde fixed HEK 293 cell. Nuclei are visualized by DAPI staining (grey). Magnified images of individual RNAs marked by dashed squares are shown on the right. Schematic position of probes shown on top. **(B)** smFISH using probes to the 5' (red) and 3' (green). **(C)** Violin plots showing distance distribution of co-localization precision of co-localizing spots from A, and 5'-3' distances for MDN1, POLA1, PRPF8 mRNAs determined by Gaussian fitting. White box plot inside the violin plot shows first quartile, median and third quartile. Median distances are shown on the right. **(D, E)** smFISH using 5' (red), 3' (red), and tiling or middle probes (cyan) respectively. **(F)** Cartoon depicting different mRNA conformations from E. **(G)** Projections of superimposed conformations from E with their centers of mass in registry, n=563. Mean Radius of gyration ($<R_g>$). Scale bars, 500 nm.

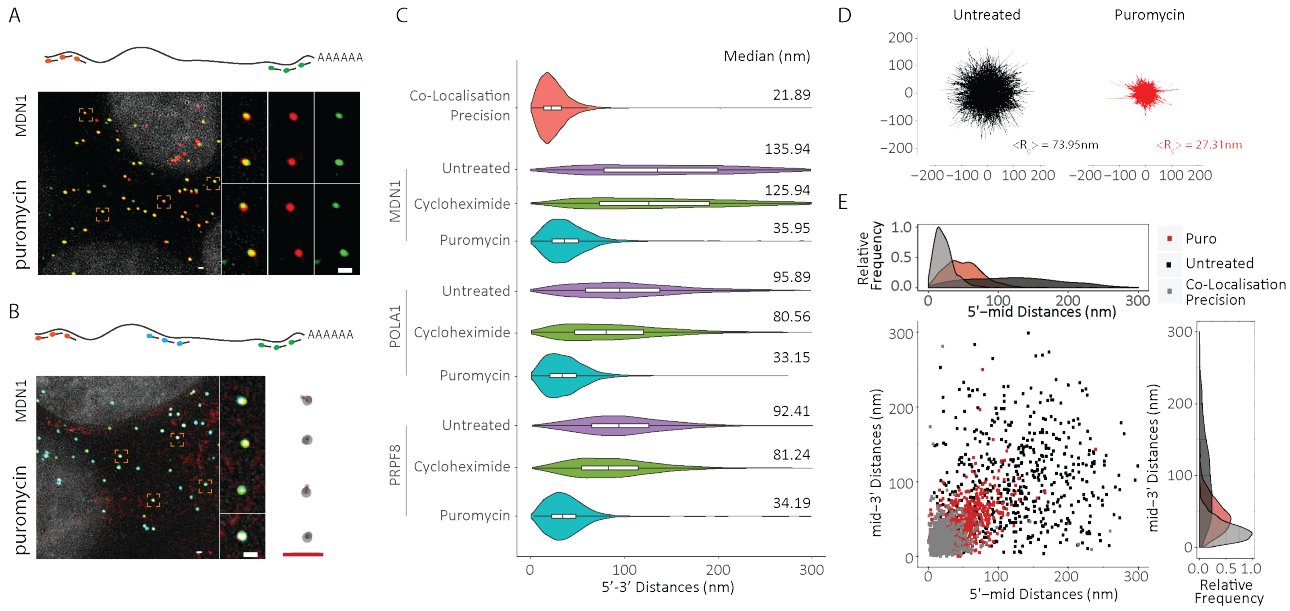

Adivarahan et al. Figure 2

Figure 2: Ribosome eviction results in mRNA compaction. (**A, B)** 5' and 3' or three color MDN1 smFISH in HEK 293 cells treated with puromycin (10 min, 100 µg/ml). **(C)** Violin plots showing 5'-3' distances for MDN1, POLA1, PRPF8 mRNAs treated with cycloheximide and puromycin. White box plot inside the violin plot shows first quartile, median and third quartile. Median distances are shown on the right. **(D)** Projections of superimposed conformations from three color MDN1 smFISH in untreated and puromycin treated cells with their centers of mass in registry, n=563. Mean Radius of gyration ($<R_g>$). **(E)** Scatter plot showing 5'mid and mid-3' distances for individual RNAs. Frequency distribution are shown on top and on the right. Scale bars, 500 nm.

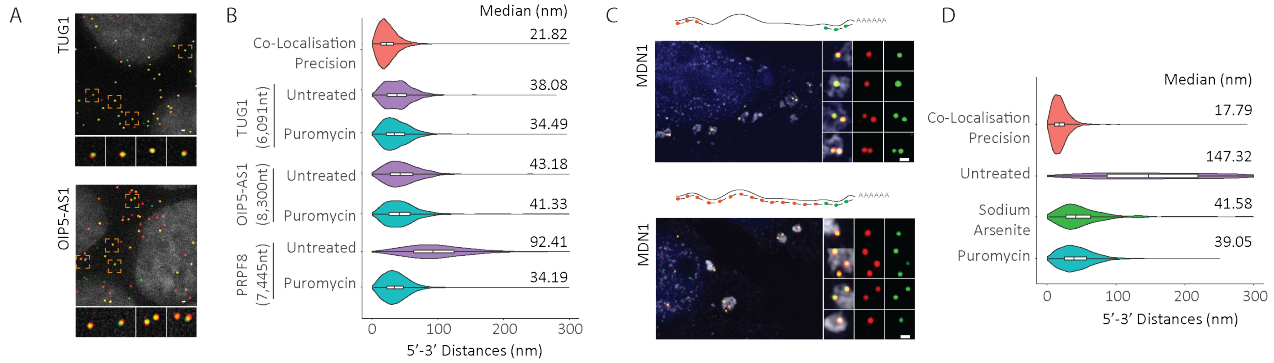

Adivarahan et al. Figure 3

Figure 3: Organization of lncRNAs and mRNAs sequestered to stress granules show compact conformations. (A) smFISH visualizing 5' and 3' ends of TUG1 and OIP5-AS1 lncRNAs. Nuclei are visualized by DAPI staining (grey). **(B)** Violin plots showing 5'-3' distance distribution of cytoplasmic TUG1 and OIP5-AS1 RNAs in untreated and puromycin treated cells compared to PRPF8 mRNAs. **(C)** 5' - 3' or 3' and tiling MDN1 smFISH in U2OS cells treated with arsenite (1 hour, 2 mM). Stress granules are visualized using an oligo dT probe (white). Nuclei are visualized by DAPI staining (blue). **(D)** Violin plots comparing MDN1 mRNA 5'-3' distance distribution for untreated, aresenite and puromycin treated cells. White box plot inside the violin plot shows first quartile, median and third quartile. Median distances are shown on the right. Scale bars, 500 nm.

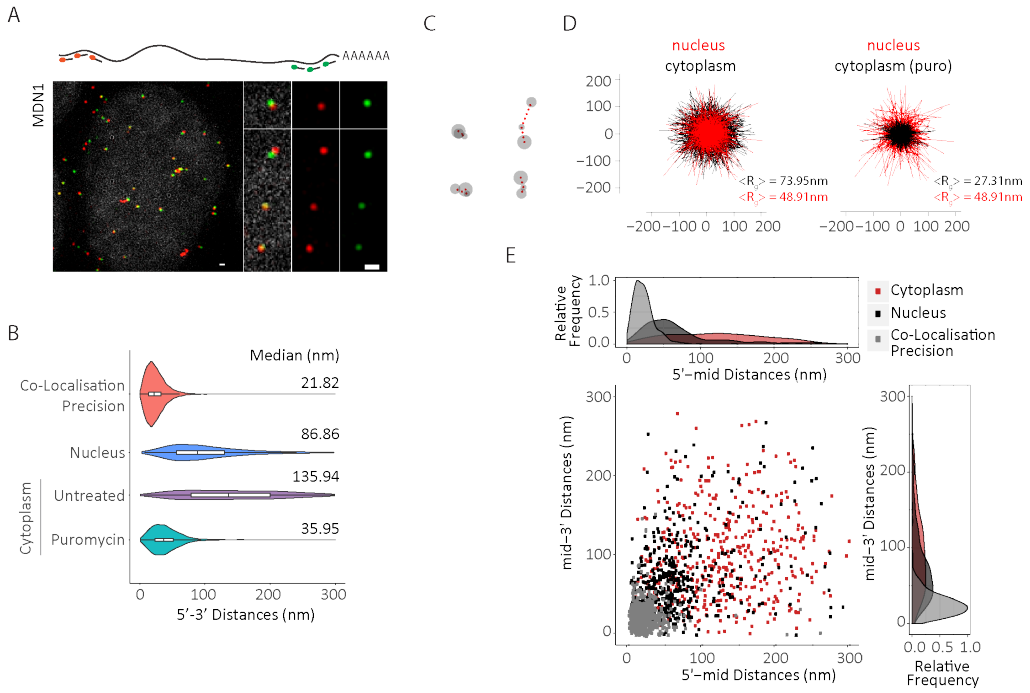

Adivarahan et al. Figure 4

Figure 4: Organization of nuclear MDN1 mRNAs. (A) 5'- 3' MDN1 smFISH of nuclear mRNAs. **(B)** Violin plots comparing MDN1 mRNA 5'-3' distance distribution of nuclear and cytoplasmic mRNAs. White box plot inside the violin plot shows first quartile, median and third quartile. Median distances are shown on the right. **(C)** Representative configurations of nuclear MDN1 mRNAs measured by 5, middle and 3' labeling as in 1E. **(D)** Projections of superimposed conformations from C with their centers of mass in registry, compared to untreated or puromycin treated cytoplasmic MDN1 mRNAs, n=452. Mean Radius of gyration ($<R_g>$). **(E)** Scatter plot comparing 5'-mid and mid-3' distances for individual nuclear and cytoplasmic MDN1 mRNAs. Frequency distribution are shown on top and on the right. Scale bars, 500 nm.